Astron. Astrophys. 282, 269–276 (1994)

ASTRONOMY AND ASTROPHYSICS

Titius-Bode laws in the solar system

II. Build your own law from disk models

B. Dubrulle[1] **and F. Graner**[2]

[1] CNRS, URA 285, Observatoire Midi Pyrénées, 14 av. E. Belin, 31400 Toulouse, France

[2] Laboratoire de Physique Statistique de l'ENS, associé au CNRS et aux Universités Paris 6 et Paris 7, 24 rue Lhomond, 75231 Paris Cedex 05, France

Received April 14, accepted July 6, 1993

Abstract. Simply respecting both scale and rotational invariance, it is easy to construct an endless collection of theoretical models predicting a Titius-Bode law, irrespective to their physical content. Due to the numerous ways to get the law and its intrinsic arbitrariness, it is not an useful constraint on theories of solar system formation.

To illustrate the simple elegance of scale-invariant methods, we explicitly cook up one of the simplest examples, an infinitely thin cold gaseous disk rotating around a central object. In that academic case, the Titius-Bode law holds during the linear stage of the gravitational instability. The time scale of the instability is of the order of a self-gravitating time scale, $(G\rho_d)^{-1/2}$, where ρ_d is the disk density. This model links the separation between different density maxima with the ratio M_D/M_C of the masses of the disk and the central object; for instance, M_D/M_C of the order of 0.18 roughly leads to the observed separation between the planets. We discuss the boundary conditions and the limit of the WKB approximation.

Key words: planets and satellites: general – solar system: general – hydrodynamics – instabilities

1. Introduction

In a previous paper (Graner & Dubrulle 1993, hereafter Paper I), symmetry considerations helped us predict that Titius-Bode laws (geometric progressions for equal phase cylinders) generically arise in scale invariant rotating systems.

From a practical point of view, however, symmetry considerations are from limited utility, since they only predict the general shape of the laws, and not its fine details (such as the value of the characteristic constants). These fine details intrinsically depend on the model considered and require explicitly solving the equations governing the system. Of course, the final result is independent of the adopted method, and brute force can be employed in any situation. However, the presence of symmetries often provides both simplification of the algebra and elegant resolution of a problem. While the presence of rotational symmetry is often taken into account when using cylindrical coordinates, scale invariance is generally ignored. As a consequence, obtaining fine details of the possible Titius-Bode law is awkward and complicated.

The aim of the present paper is twofold. First, to explicitly determine on an academic example the fine details of the laws predicted by Paper I. Second, to elegantly use the scale symmetry by introducing scale-invariant coordinates.

Among the general class of self-gravitating gaseous disks (Sect. 2), often used in previous derivations of the Titius-Bode law, we select the cold, flat self-gravitating disk (Sect. 3). This model was only chosen for its simplicity, and not because of any prejudice regarding its relevance for solar system formation. We only treat the axisymmetric case (no θ dependence); generalization to the non-axisymmetric case is possible, but tedious. We propose a set of dynamical equations, rewrite them in a scale invariant form, and perform an usual linear stability analysis (Sect. 4). We compare our results with the particular limit of the WKB approximation (Sect. 5). Endly, we present explicit recipes to "cook up" other Titius-Bode laws within maybe more realistic models, accounting e.g. for axisymmetry breaking, pressure, viscosity or finite disk thickness (Sect. 6). Our conclusion follows (Sect. 7).

2. Symmetric disk models

Planets are suspected to have formed from a primordial solar nebula. The most general equations describing such entity are:

$$\begin{aligned} \partial_t \rho + \nabla(\rho \mathbf{v}) &= 0, \\ \partial_t \mathbf{v} + (\mathbf{v}\nabla)\mathbf{v} &= -\frac{1}{\rho}\nabla P - \nabla\phi - \frac{GM_C}{r^2}\mathbf{e}_r + \nu\nabla^2\mathbf{v}, \\ \nabla^2\phi &= 4\pi G\rho. \end{aligned} \quad (1)$$

Send offprint requests to: B. Dubrulle

ρ, $\mathbf{v}$, P and ϕ are the density, velocity, pressure and self-gravitation potential; ν is the viscosity, $\mathbf{e}_r$ is the unit vector in the radial direction, M_C the mass of the central object and G the gravitational constant.

Apart from its cylindrical symmetry, the set (1) exhibits an interesting symmetry. Since it exhibits no other length scale than r itself, it is invariant under the scale transformation:

$$\begin{aligned} S_\Lambda : r &\rightarrow \Lambda r, \\ t &\rightarrow \Lambda^{3/2} t, \\ \rho &\rightarrow \Lambda^{-3} \rho, \\ v &\rightarrow \Lambda^{-1/2} v, \\ P &\rightarrow \Lambda^{-4} P, \\ \nu &\rightarrow \Lambda^{1/2} \nu, \\ \phi &\rightarrow \Lambda^{-1} \phi, \end{aligned} \tag{2}$$

where Λ is an arbitrary real number.

A system invariant through all S_Λ, Λ real, is called a scale invariant system; if a physical solution of (1) is not scale invariant, then all its transformed through the S_Λ are also solutions of (1).

It is important to point out that scale invariance is a very strong constraint, often broken by boundary conditions, pressure or viscosity prescription. For instance, if one adds to (1) the polytropic gas law:

$$P \propto \rho^\gamma,$$

the scale invariance holds if and only if $\gamma = 4/3$.

It is easy to check which extensions of the set (1) do or do not break the invariance. As for the solar or giant planet systems, most theories favor a low-mass protoplanetary disk. In that case, self-gravity is weaker than central gravity field. The motions around the central object are then approximatively Keplerian:

$$\mathbf{v} = r\Omega \mathbf{e}_\theta = \left(\frac{GM_C}{r}\right)^{1/2} \mathbf{e}_\theta, \tag{3}$$

where r is the radial cylindrical coordinate, $\mathbf{e}_\theta$ the unit vector in the azimuthal direction and Ω the Keplerian frequency. Another consequence is that along the z axis, the disk is in hydrostatic equilibrium: the pressure gradient counterbalances the gravity field projected on z; equivalently, the sound velocity c_s is simply the product of the Keplerian frequency by the height H of the disk:

$$c_s \equiv \left(\frac{dP}{d\rho}\right)^{1/2} = H\Omega. \tag{4}$$

We can conveniently define the surface and linear mass densities:

$$\begin{aligned} \sigma(r) &= \int \rho(r,z) dz, \\ \lambda(r) &= 2\pi r \sigma(r), \end{aligned} \tag{5}$$

and completely explicit the action of the scale transformation (2):

$$\begin{aligned} S_\Lambda : \Omega &\rightarrow \Lambda^{-3/2}\Omega, \\ c_s &\rightarrow \Lambda^{-1/2} c_s, \\ H &\rightarrow \Lambda H, \\ \sigma &\rightarrow \Lambda^{-2}\sigma, \\ \lambda &\rightarrow \Lambda^{-1}\lambda. \end{aligned} \tag{6}$$

3. Scale-invariant equations for the flat, cold disk

In the cold, flat, accretionless, rotating self-gravitating disk, there is no viscosity and vertical dynamics. The only physical processes are the self-gravitation competing with the stabilizing Keplerian central gravity field. This classic academic case has been frequently used in galactic dynamics, and is therefore well documented (see e.g. Fridman & Polyachenko 1984). Polyachenko & Fridman (1972) were the first to use it to explain Titius-Bode law. Their approach was however based on a two-dimensional conjugated-space treatment of the Poisson equation which dissimulates actual exponential divergences along the z axis. Here, using the scale-invariance symmetry enables us to avoid such problems.

Rather than writing the equations in coordinates (r, z, t), we introduce:

- the scale-invariant variables

$$\begin{aligned} x &= \ln(r/r_0) \\ \tau &= r^{-3/2} t, \end{aligned} \tag{7}$$

where r_0 is a still undefined normalizing radius; we refer to τ as a pseudo-time, since it is not homogeneous to a time.

- the scale-invariant functions

$$\begin{aligned} \tilde{u}(x,\tau) &= r^{1/2} v_r(r,t), \\ \tilde{v}(x,\tau) &= r^{1/2} v_\theta(r,t), \\ \tilde{\phi}(x,\tau) &= r\phi(r,t), \\ \tilde{\sigma}(x,\tau) &= r^2 \sigma(r,t), \\ \tilde{\lambda}(x,\tau) &= r\lambda(r,t). \end{aligned} \tag{8}$$

The change of variables (7) implies:

$$\begin{aligned} r\partial_r &= \partial_x - \frac{3}{2}\tau\partial_\tau, \\ \partial_t &= r^{-3/2}\partial_\tau. \end{aligned} \tag{9}$$

Since we treat here only the infinitely thin, zero temperature disk, in (1) we set $P = 0$ and $\rho(r,z,t) = \sigma(r,t)\delta(z)$, where δ is the Dirac function; so that the vertical velocity along z vanishes everywhere. The set (1) simplifies; in the plane $z = 0$, where the mass density is non-zero, it writes:

$$\partial_\tau \tilde{\lambda} - (\frac{3}{2} - \partial_x + \frac{3}{2}\tau\partial_\tau)(\tilde{\lambda}\tilde{u}) = 0, \tag{10}$$

$$\partial_\tau \tilde{u} - \tilde{u}(\frac{1}{2} - \partial_x + \frac{3}{2}\tau\partial_\tau)\tilde{u} - \tilde{v}^2 = (1 - \partial_x + \frac{3}{2}\tau\partial_\tau)\tilde{\phi} - GM_C$$

$$\partial_\tau \tilde{v} + \tilde{u}(\frac{1}{2} + \partial_x - \frac{3}{2}\tau\partial_\tau)\tilde{v} = 0. \tag{11}$$

We have not written Poisson equation, because we do not explicitly use it. Indeed, there are two main ways to treat Poisson equation. The conjugated-space treatment develops $\tilde{\sigma}$ and $\tilde{\phi}$ over a convenient set of eigenfunctions. In the usual cylindrical coordinates (r, θ, z), an obvious choice if the disk is finite is Bessel functions. Yabushita (1966, 1969) successfully applies this method to Saturn's dust ring. However, we were not able to find a set of eigenfunctions of scale-invariant coordinates which could solve Poisson equation without making the potential ϕ diverge at large scales in z.

We thus favor the real-space treatment, in which we have to evaluate ϕ only in the $z = 0$ plane, and formally treat only two-dimensional equations; we thus avoid introducing unphysical divergences. The potential $\phi(r)$ is a sum of two different contributions, from the mass distributed inside the orbit r (at a radius $R = rY$, $Y < 1$) and outside the orbit (at $R = r/Y$, $Y < 1$). We respectively note r_{min} and r_{max} the minimum and maximum radius of the disk, defined as the locations where the disk density goes to zero. They are yet unrestricted and may vary up to $r_{min} = 0$ and $r_{max} = \infty$. Using:

$$\phi(r) = -G \int_{\theta=0}^{2\pi} \int_{r=r_{min}}^{r_{max}} \frac{\sigma R dR d\theta}{(r^2 - 2rR\cos\theta + R^2)^{1/2}}, \tag{12}$$

ϕ can be written in term of the complete elliptic integral K (Gradshteyn & Ryzhik 1980), such that $2K(0)/\pi = 1$ and $K(1-\epsilon)$ diverges more slowly than $\ln(1/\epsilon)$, to obtain:

$$\begin{aligned}\phi(r) = & -G \int_{\frac{r_{min}}{r}}^{1} \lambda(rY) \frac{2K(Y)}{\pi} dY \\ & -G \int_{\frac{r}{r_{max}}}^{1} \frac{1}{Y} \lambda(\frac{r}{Y}) \frac{2K(Y)}{\pi} dY.\end{aligned} \tag{13}$$

Since $\int \lambda(R)dR$ is finite, and by definition $\lambda(r_{min}) = \lambda(r_{max}) = 0$, it is easy to check that both ϕ and $d\phi/dr$ converge. In scale-invariant notations, we simply introduce $y = \ln(Y)$, $x_{min} = \ln(r_{min}/r_0)$ and $x_{max} = \ln(r_{max}/r_0)$ and obtain:

$$\begin{aligned}\tilde{\phi}(x,\tau) = & -G \int_{x_{min}-x}^{0} \tilde{\lambda}(x+y,\tau) \frac{2K(e^y)}{\pi} dy \\ & -G \int_{x-x_{max}}^{0} \tilde{\lambda}(x-y,\tau) \frac{2K(e^y)}{\pi} e^y dy.\end{aligned} \tag{14}$$

4. Linear stability analysis

4.1. Perturbed equilibrium state

We now study the stability of the simplest scale-invariant equilibrium state, with no radial accretion ($\tilde{u} = 0$), in which the scale-invariant azimuthal angular velocity is:

$$\Omega_e^2(x) = G(M_C + M_{eg}(x)). \tag{15}$$

M_{eg} is the effective gravitational mass of the disk felt at the position x, defined as:

$$M_{eg}(x) = (\partial_x - 1)\phi_0, \tag{16}$$

where ϕ_0 is the gravitational potential defined via (14) using the equilibrium linear density $\tilde{\lambda} = L_0(x)$. Note that the gravitational disk mass M_{eg} differs from the real disk mass M_D, which is by definition (5, 8) of $\tilde{\lambda}$:

$$M_D = \int_{x_{min}}^{x_{max}} L_0(x)dx. \tag{17}$$

Perturbations around the equilibrium state will be labeled with an index 1 and with the tilde omitted. They obey the linearized equations:

$$\begin{aligned}\partial_\tau u_1 - 2\Omega_e v_1 &= (1 - \partial_x + \frac{3}{2}\tau\partial_\tau)\phi_1 \\ \partial_\tau v_1 + \frac{1}{2}(\Omega_e + \partial_x\Omega_e)u_1 &= 0 \\ \partial_\tau \lambda_1 - \frac{3}{2}L_0 u_1 + (\partial_x - \frac{3}{2}\tau\partial_\tau)(L_0 u_1) &= 0.\end{aligned} \tag{18}$$

4.2. Boundary conditions

The resolution of such problem of course depends on boundary conditions. The most natural are $\lambda_1(x_{min}) = \lambda_1(x_{max}) = 0$.

As usual, the stability analysis is simplified with the use of a set of eigenfunctions of the problem. In the present case, the scale invariance translates into a translation invariance for the variable x. A natural choice of eigenfunctions is therefore the set of Fourier modes

$$\{\Psi_k(x) = \exp[ikx];\ k = nk_0;\ |n| = 0, 1, 2...\},$$

where k_0 is the fundamental wavenumber:

$$k_0 = \frac{\pi}{x_{max} - x_{min}} = \frac{\pi}{\ln(r_{max}/r_{min})}. \tag{19}$$

The boundary conditions are then satisfied provided either $r_0 = r_{min}$ or $r_0 = r_{max}$. The solutions of (18) will then be expressed as linear combinations of $\sin(nk_0x)$.

4.3. Coupling between modes

Once the equilibrium density $L_0(x)$ has been specified, the stability analysis can be performed via a decomposition of both equilibrium and perturbed quantities on the set of eigenfunction, and then projection of the Eqs. (18) on each mode. In general, the resulting equations couple modes with different wavenumbers via (i) cross terms like L_0u_1 or $\Omega_e v_1$, or (ii) edge effects such as in $M_{eg}(x)$; or $\phi_1(x)$, since the bounds in the integral also depend on x.

The type (i) couplings disappear in the special case $L_0(x) = L = cst$. This case corresponds to a surface density decreasing like r^{-2}. It is the only solution of (1) which is scale-invariant. From the planetologist point of view, such solution has no special significance, although it is favored by some time scale arguments regarding planet formation (Lissauer 1987). From our point of view, it is just a convenient case, because it leads to a mode decoupling and makes the computations much simpler. Any real Titius-Bode hunter should consider starting with more

realistic density distributions, e.g. in order to get constraints on their shape and amplitude. As explained in the conclusion, however, we do not encourage anyone to try this direction.

The type (ii) couplings formally disappear when $r_{min} = 0$ and $r_{max} = \infty$. Such case has no physical significance, especially for simple monotonic surface density $\sigma(r)$, because it implies considering a disk with infinite mass. Physically, it corresponds to the idealized "large box" approximation, in which the Fourier modes become continuous ($k_0 \to 0$). In our case, we do not directly use this limit, because of the divergence involved on the disk mass M_D. However, we indirectly use it by noting that, formally, the density is zero outside $[r_{min}, r_{max}]$. We can therefore extend to 0 the lower limit in both integrals involved in (13) or equivalently to $-\infty$ in (14): we only have to multiply their integrand by a weight function, which cuts off contributions corresponding to low or high r. The simplest weighting procedure which preserves the scale invariance and decouples modes only substitutes to $K(y)$ in (13) the function $K(y)-K(0)$. This is an approximation, because the corresponding cut off formally occurs only at $r = 0$ and $r = \infty$. We therefore expect this approximation to work at best in the local approximation ($k \gg 1$) where the location of the boundaries is irrelevant.

4.4. Decoupled modes

With these two assumptions, both the gravitating disk mass M_{eg}, and the k Fourier component ϕ_k of the first order potential ϕ_1, take very simple expressions:

$$\begin{aligned} M_{eg} &= LN(0), \\ \phi_k &= -GN(k)\lambda_k, \end{aligned} \tag{20}$$

where λ_k is the k Fourier component of λ_1, L the constant scale-invariant equilibrium density and $N(k)$ the complex non-dimensional form factor:

$$\begin{aligned} N(k) = &\int_{-\infty}^{0} e^{iky} \frac{2(K(e^y) - K(0))}{\pi} dy \\ &+ \int_{-\infty}^{0} e^{(1-ik)y} \frac{2(K(e^y) - K(0))}{\pi} dy. \end{aligned} \tag{21}$$

The appendix develops a convenient approximation of $N(k)$, valid for all k. Its main properties are $N(0) = 2\ln 2 - 1 \sim 0.39$ (see Gradshteyn & Ryzhik 1980, formulae 6.141 and 6.142) and $N(k) \sim |k|^{-1} - 0.5\, ik^{-2}$ for large k (see appendix). Note also that the effective gravitational mass and the actual disk mass are related via the fundamental (smallest) wave number k_0, as defined in (19):

$$\frac{M_{eg}}{M_D} = \frac{N(0)k_0}{\pi}. \tag{22}$$

In the following, we only use the effective gravitational mass M_{eg}, because it is independent of the location of the boundaries. However, when typical numerical values are needed, we choose the value of M_{eg} so that, for $r_{max}/r_{min} = 100$ (approximatively the ratio of Pluto perihelion to Mercury perihelion), or equivalently $k_0 = 0.68$, it corresponds to $M_D/M_C = 1$, $M_D/M_C = 0.3$ and $M_D/M_C = 0.03$. The first case is typical of a disk around a TTauri star; the second is the largest disk which is stable with respect to the gravitational instability studied by Shu et al. 1990; the last case corresponds to the minimum solar nebula, estimated with all planetary masses spread up to Pluto's orbit, and augmented up to solar composition (Kuiper 1951; Prentice 1977). Translated into M_{eg}, the three cases lead respectively to $M_{eg}/M_C = 8.4 \times 10^{-2}$, 2.5×10^{-2} and 2.5×10^{-3}.

4.5. Temporal stability

In the formulation we adopted, the stability analysis becomes especially simple. All the modes decouple; the evolution of a given k component obeys the equations:

$$\partial_\tau \begin{bmatrix} u_k \\ v_k \\ l_k \end{bmatrix} = \frac{1}{\Delta} \begin{bmatrix} \Omega_k^2 T(ik - \frac{3}{2}) & 2\Omega_e & \Omega_k^2(ik-1) \\ -\frac{1}{2}\Omega_e \Delta & 0 & 0 \\ -(ik - \frac{3}{2}) & 2\Omega_e T & \Omega_k^2 T(ik-1) \end{bmatrix} \begin{bmatrix} u_k \\ v_k \\ l_k \end{bmatrix} \tag{23}$$

where we use the following notations:

$$\begin{aligned} l_k &= \lambda_k / L, \\ \Omega_e^2 &= G(M_C + M_{eg}), \\ \Omega_k^2 &= GLN(k), \\ T &= 3\tau/2, \\ \Delta &= 1 + \Omega_k^2 T^2. \end{aligned} \tag{24}$$

Note that our scale-invariant notations have the following physical dimensions:

$$\begin{aligned} u_1, v_1, \tau^{-1}, T^{-1}, \Omega_e, \Omega_k &\to [meter]^{3/2} \times [second]^{-1}, \\ \phi_1, GM_C &\to [meter]^3 \times [second]^{-2}, \\ L, \lambda_k, M_C, M_{eg} &\to [kg], \\ k, x, l_k, N(k), \Delta &\to dimensionless. \end{aligned} \tag{25}$$

As a consequence of scale-invariance, the stability problem is explicitly pseudo-time dependent. As we see below, this allows for both exponentially and algebraically growing instabilities. We search for the perturbed quantities a pseudo-time dependence:

$$(u_k(\tau), v_k(\tau), l_k(\tau)) = e^{\int_0^\tau \omega_k(s)ds} (u_{0k}, v_{0k}, l_{0k}). \tag{26}$$

Therefore, the system is stable (resp. unstable) at the pseudo-time τ_0 if the real part of $\int_0^{\tau_0} \omega_k$ is positive (resp. negative). Using (23), it appears that ω_k is one of the eigenvalues of the 3×3 matrix and satisfies:

$$\begin{aligned} &\omega_k = 0, \quad \text{or} \quad \omega_k^2 \Delta + \Omega_k^2 T(\frac{5}{2} - 2ik)\omega_k \\ &+[\Omega_e^2 + (\frac{3}{2} - \frac{5}{2}ik - k^2)\Omega_k^2] = 0. \end{aligned} \tag{27}$$

The neutral mode ($\omega_k = 0$) is linked with our description of the system as dissipationless: as soon as viscosity is included, this mode steadily decays over a viscous time scale. The two other modes solutions of (27) determine the stability of the system.

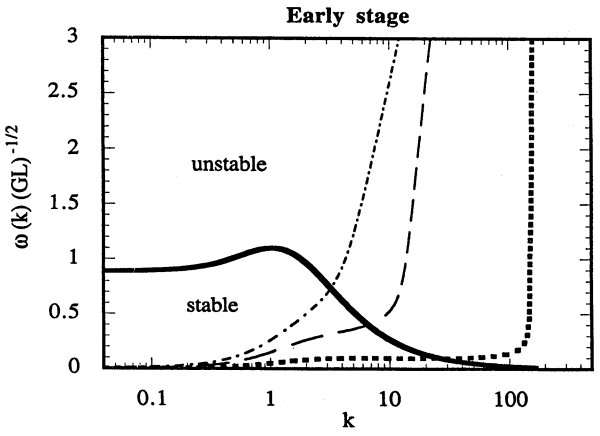

Fig. 1. Growthrate of instability as a function of the wavenumber k, for the flat disk problem, at the early stage of the evolution, and for various values of the ratio M_{eg}/M_C: $M_{eg}/M_C = 8.4 \times 10^{-2}$ (dashed dot line); $M_{eg}/M_C = 2.5 \times 10^{-2}$ (dashed line); $M_{eg}/M_C = 2.5 \times 10^{-3}$ (dotted line). The growthrate ω is expressed in units of $(GL)^{1/2}$. Solid line marks the critical growthrate ω_c below which the late stage is algebraically stable

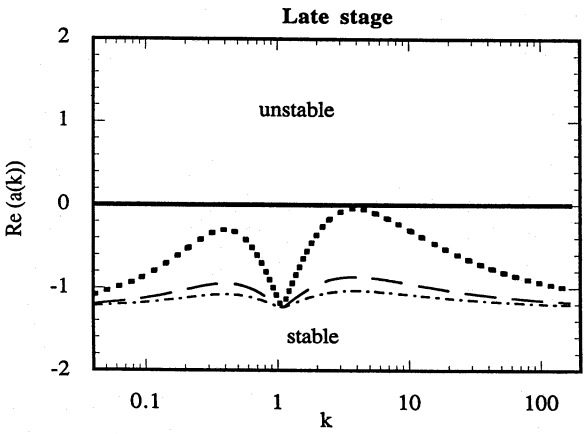

Fig. 2. Exponent a of the power law in the late stage of the evolution, as a function of the wavenumber k and for various ratios M_{eg}/M_C: $M_{eg}/M_C = 8.4 \times 10^{-2}$ (dotted line); $M_{eg}/M_C = 2.5 \times 10^{-2}$ (dashed line); $M_{eg}/M_C = 2.5 \times 10^{-3}$ (dashed dot line)

4.6. Early stage

In the early stage ($|\Omega_k|\tau \ll 1$) of the evolution, ω_k is solution of:

$$\omega_k^2 + \Omega_e^2 + (\frac{3}{2} - \frac{5}{2}ik - k^2)\Omega_k^2 = 0. \quad (28)$$

Eq. (28) is characterized by the absence of terms linear in ω_k. Moreover, the imaginary part of the term independent of ω_k is not zero. Therefore, at any wavenumber, one of the two solutions of (28) has a positive real part, i.e. the system is unstable for any k during the early stage.

Figure 1 shows the variation with k of the real part of the unstable solution of (28) expressed in units of $\sqrt{GL}$, for various values of the ratio M_{eg}/M_C. The time scale of this early-stage instability is quite different for high and low wavenumbers: low wavenumber modes are slowly growing ($Re(\omega_k) < \sqrt{GL}$), while higher wavenumber modes are much more unstable. The transition between the two regimes is characterized by a "bend" in the curve $\omega(k)$, which occurs at a critical wavenumber k_c. Visual inspection of Fig. 1 gives k_c of the order of 5 to 20 for both massive disks and 150 for the low mass disk (respectively $M_{eg}/M_C = 8.4 \times 10^{-2}$; 2.5×10^{-2}; 2.5×10^{-3}).

4.7. Late stage

In fact, as we now show, this critical wavenumber marks the transition between the stable and unstable regime, because low wavenumber modes are stable at later stages of the evolution ($|\Omega_k|\tau \gg 1$). For such low wavenumbers, the late stage behavior is algebraic instead of exponential: $\omega_k \sim a/\tau$ to lowest order in $1/\tau$, i.e. the perturbed quantities go like τ^a, where the exponent a of the power law obeys:

$$a^2 + (\frac{5}{2} - 2ik)a + \frac{\Omega_e^2}{\Omega_k^2} + \frac{3}{2} - \frac{5}{2}ik - k^2 = 0. \quad (29)$$

The real part of the solutions of such equation is always negative, as shown in Fig. 2 for various disk masses. The perturbations undergo a power-law decay, therefore low wavenumbers are algebraically stable ar large τ.

Of course, this argument is relevant only if the system never leaves the linear regime, i.e. if the initial infinitesimal perturbations never reach relative amplitude of order unity. To estimate which wavenumbers are likely to stay in the linear regime, we may proceed as follow: the early stage evolution is valid roughly up to a pseudo-time $\tau_0 = |\Omega_k|^{-1}$, after which the late stage description (algebraic decay) becomes relevant. During this time, a perturbation increases by a factor of order of $\exp[Re(\omega_k)_{\tau=0}|\Omega_k|^{-1}]$. We now decide that this increase is sufficient to make the perturbation non-linear provided the factor of increase is larger than 10, so that the perturbation has grown by more than an order of magnitude. This is a rather crude criterion, but it enables to get the order of magnitude of the critical wavenumber. We therefore get a rough criterion for validity of the late stage description, which defines ω_c:

$$Re(\omega_k)_{\tau=0} < \omega_c \equiv |\Omega_k| \ln 10. \quad (30)$$

The curve $\omega_c(k)$ has also been drawn in Fig. 1. It delimitates the linearly stable and unstable regimes. The critical wavenumber for stability k_c can then be computed more precisely as the crossing between the dispersion relation $\omega(k)$ and the critical curve $\omega_c(k)$: by definition of k_c, $\omega_c(k_c) = \omega(k_c)$. We respectively find $k_c = 3.2,\ 6.69,\ 26.66$ for $M_{eg}/M_C = 8.4 \times 10^{-2},\ 2.5 \times 10^{-2},\ 2.5 \times 10^{-3}$, which confirms our previous estimate based on a visual inspection of Fig. 1. We have also computed the ratio M_{eg}/M_C for which $k_c = 11.8,\ 13.4,\ 15.5$ and 18.7 (see

discussion): it is respectively $M_{eg}/M_C = 0.01,\ 0.008,\ 0.007$ and 0.005.

5. Comparison with WKB analysis

It is interesting to compare this stability analysis with the usual WKB analysis. In scale invariant variables, it is easy to check that the WKB approximation corresponds to $k \gg 1$ and $\tau = 0$. Within these two limits, our equations (21, 24, 27) reduce to:

$$\Omega_k^2 = GL|k|^{-1}, \tag{31}$$

$$\omega_k^2 + \Omega_e^2 - GL|k| = 0. \tag{32}$$

Equation (32) is obviously the scale invariant equivalent of the well-known dispersion equation (Fridman & Polyachenko 1984):

$$\omega^2 + \Omega(r)^2 - 2\pi G\Sigma(r)|k(r)| = 0, \tag{33}$$

since $\omega_k^2 = r^3\omega^2$, $\Omega_e^2 = r^3\Omega^2(r)$, $k = rk(r)$ and $L = 2\pi r^2\Sigma(r)$.

In the approximation (32), the disk is stable for low wavenumbers and unstable for wavenumbers larger than the threshold k_{WKB} which writes, in our notations:

$$k_{WKB} = \frac{\Omega_e^2}{GL} = N(0)(1 + \frac{M_C}{M_{eg}}). \tag{34}$$

Such wavenumber corresponds to the location of the"bend" observed in Fig. 1. More precisely, it is respectively $k_{WKB} =$ 5, 16, 156 for $M_{eg}/M_C = 8.4\times10^{-2};\ 2.5\times10^{-2};\ 2.5\times10^{-3}$. Such small-scale, early-stage analysis is compatible with ours for massive disks, and is oversimplified for light disks, large scales or late stage.

6. Discussion

6.1. Derivation of a Titius-Bode law

Low wavenumbers are linearly stable; while large wavenumbers are linearly unstable and enter a (potentially stabilized) non-linear regime. Our analysis does not investigate the selection of a particular wavenumber amongst all the unstable modes. Titius-Bodes hunters may favor the following back-of-the-envelope calculation. The only typical length scale of our idealized flat disk originates from k_c. Since the structure of the solutions to (23) are proportional to $\sin(k_c x)$ the density extrema increase geometrically with r:

$$\frac{r_{n+1}}{r_n} = \exp[2\pi/k_c]. \tag{35}$$

If these extrema corresponded to the sites of planet formation, the observed planetary distances distribution (see introduction) would obey:

$$k_c = \frac{2\pi}{\ln(K)}, \tag{36}$$

i.e. $k_c = 11.8$ for the solar system, or $k_c = 13.4,\ 15.5$ and 18.7 for the satellite system of respectively Jupiter, Saturne and Uranus. This is achieved respectively for $M_{eg}/M_C = 0.01$ (solar system), 0.008, 0.007 and 0.005 for the Jupiter, Saturne and Uranus system. Assuming that the initial disk was extending between the innermost and outermost planet or satellite, we approximatively get $r_{max}/r_{min} = 100$ for the solar system, and $r_{max}/r_{min} = 25$ for the disks around giant planets. The observed Titius-Bode laws are then recovered, provided the mass of the initial disks were respectively $M_D/M_C = 0.18$ (sun), 0.07 (Jupiter), 0.06 (Saturne) and 0.04 (Uranus). However, this is a rather cheap way to obtain a Titius-Bode law.

6.2. Elaborate models

Indeed, many more complex linear or non-linear models, e.g. mentioned in Paper I, also lead to Titius-Bode type laws. In any disk, non-linearities introduce characteristic length scales and the resulting k is a priori very far from k_c. Even within the linear regime, more realistic boundary conditions would select a different mode. Moreover, the actual selection of the instability wavelength probably arises from the competition with another physical mechanism, which result in a maximum in the dispersion relation $\omega(k)$, i.e. a mode growing faster than the others. A typical example is the viscous stabilization of large k.

Such processes can be included in the type of model described here without breaking the Titius-Bode law, provided they respect the scale invariance (2,6). Explicit recipes to cook up a more complex Titius-Bode law include a vertical scale height $H \propto r$, a temperature profile $T \propto r^{-1}$, a turbulent viscosity $\nu_t = \alpha c_s^2/\Omega$ with α constant and $c_s \sim r^{-1/2}, r^{-2}$ force fields, a vortex size $\propto r$, a state equation $P \propto \rho^{4/3}$, a constant Mach number, etc... Therefore, the possibilities of cooking up Titius-Bode laws are endless and only restricted by our own imagination.

6.3. Axisymmetry breaking

Non axisymmetry and z dependence can also be included, at the price of adding to (7) the two scale-invariant variables θ and $\zeta = z/r$. Breaking the rotational invariance is as rich as breaking the scale invariance. For instance, the first azimuthal deformation mode $m = 2$ corresponds to an elliptical structure; a fundamental $m = 2$ and smaller contributions from modes with high, even values of m lead to a bar i.e., in a rotating disk, to a barred spiral. Asteroid belt or giant planet annuli are axisymmetric; on the opposite, planets and satellites are Dirac peaks $\delta(\theta)$, or at least correspond to high, odd values of m azimuthal modes.

Note that the decoupling (P4) we assumed in Paper I between radial and azimuthal perturbations is effective in at least one simple case. A particle placed at a radius r feels an axisymmetric gravitation force from an annulus of matter, even inhomogeneous, placed at a different radius r', provided the annulus rotates relatively to the particle. For small k (r' far from r) the relative angular rotation is of order of the keplerian frequency. Setting aside resonance effects, the rotation of the annulus averages out the variations of the force it exerts, if there is a large

number of rotations during the azimuthal accretion stage. The self-gravitation sets the typical radial instability pseudo-time scales $|\Omega_k|^{-1}$. The validity criterion is thus $|\Omega_k| \ll \Omega_e$, ie the disk mass is not much larger than the instability threshold.

Current theories of planet formation favor growth of planets or satellites via coagulation of larger and larger particles, i.e. instability of very large k. On the other hand, models of formation of protoplanets and protosatellites through self-gravitation based on the Titius-Bode law set the constraint $11.8 < k < 18.7$. Both types of theories are compatible if a gravitational instability first created denser annuli obeying a Titius-Bode law, followed by particles coagulation within these annuli. Such scenario requires rather massive disks to start with (M_D of the order of a few tenth the mass of the central object, from our analysis). The uncertainities governing the current theories of planetary systems formation are too large to rule out such results. In the case of the solar system, however, this result corroborates the conclusions obtained via turbulent disk models (Dubrulle 1993).

7. Conclusion

Noting that gravitation sets no intrinsic length scale, due to its infinite range, we explain how to obtain scale-invariant equations on the simplest example of a self-gravitating disk. We use them for a complete linear stability analysis, compatible with existing models of protoplanetary disks. We compute the critical wavenumber above which self-gravitation instabilities can develop and show density maxima positions r_n obey a Titius-Bode law: $x_n = \ln(r_n/r_0) = 2n\pi/k = n\ln(K)$.

Our study shows that there are potentially an infinite number of ways of obtaining Titius-Bode laws, providing one strictly sticks to processes which do not break the scale invariance. Thus K is extremely sensitive to various parameters such as disk mass, radial and vertical density distribution, but also boundary conditions, viscosity, temperature, or chemical composition. Obviously, the single (and controverted) present value of K (≈ 1.7 for the solar system) can not even give access to the mass of the original disk.

In conclusion, linear or non-linear Titius-Bode laws can now be firmly considered as at worst numerology, at best an outcome of some simple symmetries; but even the value of the constant K does not set any relevant constraint on cosmogonic models of solar system formation.

Acknowledgements. We thank B. Janiaud, A. Chiffaudel and R. Lehoucq for critical reading of the manuscript. This work was supported by the Programme National de Planétologie.

Appendix

In this appendix, we build a convenient approximation to the form factor $N(k)$; the quality of the approximation will be checked by comparison with a numerical value, obtained by direct integration of (21).

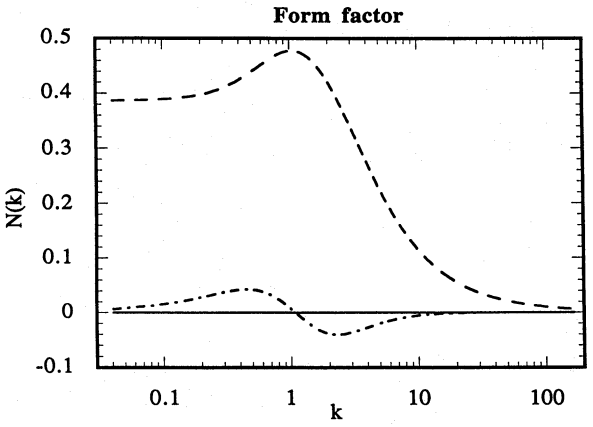

Fig. 3. Real (dashed line) and imaginary (dashed dot line) part of the form factor $N(k)$ given by (41), as a function of the wavenumber, k

Table 1. Form factor N: comparison between the exact numerical integration of (21), label *num*, and its analytical approximation (41), label *appr*. Note the good agreement at small k, and the large-k variation $Re(N) \sim |k|^{-1}$, $Im(N) \sim -k^{-2}$.

k	$N(k)_{num}$	$N(k)_{appr}$
0	$2\ln 2 - 1 = 0.39$	0.38
10	$0.15 - 0.008\,i$	$0.1 - 0.005\,i$
100	$0.015 - 0.00008\,i$	$0.01 - 0.00005\,i$

As a first step, we checked numerically that over the range $[0, 0.99]$ the elliptic integral $K(y)$ can be approximated, within a few percent, by:

$$K(y) = K(0) - 0.5\,y\ln(1-y). \tag{37}$$

Therefore, we approximatively write:

$$N(k) = -0.5\int_{-\infty}^{0} e^{(ik+1)y}\frac{2\ln(1-e^y)}{\pi}dy - 0.5\int_{-\infty}^{0} e^{(2-ik)y}\frac{2\ln(1-e^y)}{\pi}dy. \tag{38}$$

Both integrals are dominated by the contribution around $y = 0$, where the integrand becomes singular. In this neighborhood, $\ln(1-e^y) \sim \ln(-y)$. Since it brings the largest contribution, we use $\ln(-y)$ as an approximation of $\ln(1-e^y)$ in the equation (38). After a change of variable $v = -y$, we therefore obtain:

$$N(k) = -0.5\int_{0}^{\infty} e^{-(ik+1)v}\frac{2\ln(v)}{\pi}dv - 0.5\int_{0}^{\infty} e^{-(2-ik)v}\frac{2\ln(v)}{\pi}dv. \tag{39}$$

The two integrals can be computed exactly, using (Gradshteyn & Ryzhik 1980), formula 4.331):

$$\int_0^\infty e^{\mu v}\ln(v)dv = -\frac{1}{\mu}(\mathbf{C} + \ln\mu),\ [Re(\mu) > 0], \tag{40}$$

where $\mathbf{C} = 0.577$ is Euler's constant. We recall that the notation $\ln(z)$ when $z = |z|e^{i\theta}$ is a complex number stands for $\ln(|z|)+i\theta$.

We obtain the following approximation for $N(k)$:

$$N(k) = \frac{1}{\pi}\left(\frac{\mathbf{C} + \ln(1+ik)}{1+ik} + \frac{\mathbf{C} + \ln(2-ik)}{2-ik}\right). \quad (41)$$

The real and imaginary part of $N(k)$ obtained from (41) are plotted in Fig. 3. Table 1 shows the comparison between this analytical, approximated expression of $N(k)$ and a few exact, numerically integrated values. The approximation (41) is satisfactory for our purpose.

Thanks to this approximation, the asymptotic value of $N(k)$ can be found via a simple expansion. We find:

$$N(k) = \frac{1}{|k|} - \frac{i}{2k^2}, \quad |k| \gg 1. \quad (42)$$

References

Dubrulle, B.: 1993, Icarus in press

Fridman, A. and Polyachenko, V.: 1984, *Physics of gravitating systems*, Springer

Gradshteyn, I. and Ryzhik, I.: 1980, *Table of integrals, series and products. Corrected and enlarged edition*, Academic Press, New York

Graner, F. and Dubrulle, B.: 1993, A&A companion paper

Kuiper, G.: 1951, ApJ **109**, 308

Lissauer, J.: 1987, Icarus **69**, 249

Polyachenko, V. and Fridman, A.: 1972, Sov. Astron. **16**, 123

Prentice, A.: 1977, in S. Dermott (ed.), *The Origin of the Solar System*, Wiley, New York

Shu, F., Tremaine, S., Adams, F., and Ruden, S.: 1990, ApJ **358**, 495

Yabushita, S.: 1966, MNRAS **133**, 247

Yabushita, S.: 1969, MNRAS **142**, 201

This article was processed by the author using Springer-Verlag LaTeX A&A style file version 3.